Erosion-corrosion behaviour of $CoCrFeNiMo_{0.85}$ and $Al_{0.5}CoCrFeNi$ complex concentrated alloys produced by laser metal deposition

Frazer Brownlie[1], Trevor Hodgkiess[1], and Francesco Fanicchia[2]*

[1] Weir Advanced Research Centre, Glasgow, UK, G1 1RD

[2] TWI Ltd, Granta Park, Cambridge, UK, CB21 6AL

** Correspondance: Frazer.Brownlie@mail.weir*

Abstract

This study evaluates the corrosion and erosion-corrosion behaviour of two complex concentrated alloys (CCAs), $CoCrFeNiMo_{0.85}$ and $Al_{0.5}CoCrFeNi$, deposited by Laser Metal Deposition (LMD) onto a stainless steel substrate. The performances of the CCAs were compared to wrought stainless steel (UNS S30403) and carbon steel (P265GH). Erosion-corrosion testing was conducted using a submerged impingement jet test rig utilising a slurry comprising angular silica sand in an aqueous solution of 3.5%NaCl, adjusted to a pH of 4, impinging at 90°. Electrochemical monitoring was also undertaken in quiescent, flowing and solid-liquid conditions. The microhardness of $CoCrFeNiMo_{0.85}$ was observed to be significantly greater compared to $Al_{0.5}CoCeFeNi$ due to the presence of intermetallic phases (identified by XRD) in the former. Although the $CoCrFeNiMo_{0.85}$ CCA generally demonstrated superior durability than the $CoCrFeNiMo_{0.85}$ variant, the relative performances of the investigated materials were observed to be dependent upon the hydrodynamic conditions. An important factor was the complex influence of corrosion on the overall erosion corrosion process. Indeed, when cathodic protection was applied, less distinct differences between the investigated alloys were evident in terms of the resulting pure mechanical damage. Post-test microscopy using SEM demonstrated that both CCAs experienced similar mechanical degradation mechanisms – sliding abrasion in low angle conditions and plastic deformation and micro-cracking in high angle conditions.

Keywords: Compositionally complex alloys, erosion-corrosion, polarisation, laser metal deposition

1. Introduction

The field of High Entropy Alloys (HEA) represents a new approach to alloy development that has emerged in the last 10 – 20 years. Such alloys comprise at least 5 major constituents at or near, equal atomic % ("equimolar") concentrations [1] and the original aim was to achieve extensive single-phase solid solutions in which the disordered arrangements of the constituent metals constitute a thermodynamic state of high entropy. Subsequent developments comprised the production of multiphase structures containing some constituents present at non-equimolar concentrations, thus significantly extending the potential range of alloy compositions [2, 3]. This has led to the use of an alternative description of such alloys: "complex concentrated alloys" (CCAs), which is the term used throughout this work.

The exploitation of this new class of materials clearly must be based on a detailed appreciation of the relationships between their structures and properties and comprehensive general reviews of these aspects are available in the literature - of which examples are [1-4]. Early investigators focused on the mechanisms whereby such CCAs provided extremely high strengths, also maintained up to higher temperatures than conventional materials based on perhaps one or two elements present in major proportions. Also, other desirable properties – often relating to specific alloy compositions – have been assessed. These include, for instance, toughness and the often-elusive combination of high strength and toughness [5]. Subsequently, the characteristics of CCAs in yielding improvements in a range of other material properties including fatigue, magnetic properties, corrosion behaviour [4] have been probed.

CCAs can be produced in "bulk" form by a number of processes (such as arc melting and casting, mechanical alloying, powder metallurgy) and they may be required in such condition

for many applications. The potential of additive manufacturing for application to high-entropy alloys is also being explored [6]. Where the properties of surfaces are important, however, the use of these new alloys in the form of coatings is clearly an attractive option. Candidate coating processes such as thermal spraying, vapour deposition [7], magnetron sputtering [8] and laser cladding have been tested [9, 10]. With such an approach, the surface engineering performance of a low-grade material – such as carbon steel - can be most effectively and economically improved. Two crucial surface engineering properties, required in many engineering applications, are resistance to corrosion and to various types of wear damage. The CCA coatings synthesised by laser cladding, electro-spark deposition, and magnetron sputtering involve rapid-cooling processes which contributes to a homogeneous coating structure which should result in good corrosion resistance [11].

Since many of the CCAs contain corrosion resistant elements, such as chromium and molybdenum at elevated concentrations compared to traditional corrosion-resistant alloys (e.g. Ni-base and stainless steels), CCAs clearly have potential to confer superior corrosion resistance. Nevertheless, careful consideration of the overall constitution of such CCAs is necessary [11] in order to avoid elemental segregation interrupting the formation of uniform passive films upon which the corrosion resistance depends. This aspect has received significant attention in the past. Ayyagari et al. [8] found that the pitting resistance in 3.5% NaCl solution of as-cast and recrystallised $Al_{0.1}$CoCrFeNi was superior to that of UNS S30400 stainless steel. Other workers [12] have reported similar relative behaviour of this CCA (in arc melted/hot isostatic pressed condition) compared to UNS S31603 alloy. Zhang et al. [9] also report a substantially superior corrosion resistance of FeCoCrAlNi CCA coating in 3.5% NaCl solution compared to that of UNS S30400 stainless steel. Another laser-clad Cr-containing CCA (CrMnFeCoNi), exhibited passive behaviour in 3.5% NaCl solution but appeared to possess reduced resistance to pitting than UNS S30400 [13]. Comparisons of a large number of CCA alloys with some common conventional alloys demonstrated [14] a

systematic improvement in corrosion resistance in NaCl solution compared to mild steel but variable performance when compared to ferritic and austenitic stainless steel UNS S30400.

The search for improved surface engineering properties extends to wear, erosion and corrosive-wear behaviour – especially as the common traditional materials, carbon steels, and stainless steels, are well-known to possess limited resistances in such conditions. Increases in wear resistance are frequently related (at least qualitatively) to material hardness. Thus dry, ball-on-disc tests on thin (5 μm) multicomponent (Ti-Hf-Zr-V-Nb) nitride coatings indicated superior wear performance than exhibited by a 1045 steel substrate [7]; the improvement being attributed to the measured higher hardness of the coated material. Nevertheless, in connection with conventional materials at least, such simple correlations are rarely observed – especially in connection with erosive wear. Expanding the association of wear behaviour with alternative mechanical properties, such as elastic modulus and fracture toughness, is also an uncertain strategy on account of the much higher strain rates associated with solid particle erosion than those used in the measurement of basic mechanical properties of materials. These uncertainties are accentuated when attention is turned to CCAs on account of the scarcity of mechanical property data for these complex alloys. As pointed out by George et al. [15] mechanical property data for such materials is currently largely limited to uniaxial tension/compression conditions. Only limited information is available for other loading conditions, such as fatigue, fracture toughness and work hardening during plastic deformation, that are likely to be relevant under erosive attack. Factoring in the influence of a corrosive environment introduces yet further complications. Thus, “extrapolation” of satisfactory corrosion resistance, observed in quiescent conditions with many CCAs, cannot be transferred to predict behaviour in corrosive wear situations on account of the complex, interactive (“synergistic”) processes that are routinely present during such deterioration. Consequently, prediction of the behaviour of CCAs, for instance in erosion-corrosion systems, must be based on experimental investigations.

Although some effort has been expended on these aspects, in fact very little attention has been focused on corrosive wear and erosion-corrosion. The cavitation erosion resistance of AlCoCrFeNiTi coatings was observed [16] to be reduced in 3.5% NaCl solution compared to distilled water – undoubtedly due to the role of corrosion on the behaviour in these situations. In one study [9] the cavitation erosion of FeCoCrAlNi CCA coating in 3.5% NaCl solution was observed to be 7.6 times better that that of 304 stainless steel. The important feature of CCA constitution was demonstrated in a study [10] of the influence of the aluminium content in laser-clad AlxCoCrFeNiTi0.5 on the slurry erosion behaviour in an unspecified aqueous solution. The slurry erosion resistance of CCA Al0.1CoCrFeNi was found [17] to be superior to that of mild steel but lower than UNS S31603 stainless steel but these comparisons relate mainly to mechanical damage as the test programme was carried out in a tapwater slurry. A detailed comparison [18], of the corrosion and erosion-corrosion behaviour of a $Al_{0.1}$CoCrFeNi CCA alloy and conventional UNS S31603 stainless steel in a 3.5% NaCl slurry, revealed that the material loss of the CCA alloy was slightly greater than that of the stainless steel at an impingement angle of 90° but much less at 30° impact – mainly on account of a considerable increase in material loss of the stainless steel at the oblique angle. Although the work described in this paper [18] covered an interesting range of aspects, the paper suffers somewhat in a number of respects such as corrosion monitoring exercises not including in-situ measurements, failure to separate synergy into its two erosive and corrosive components and a misinterpretation of the role of the squeeze film in erosion-corrosion systems.

It is clear that there is a need for further attention on the overall corrosive wear behaviour of CCAs. Specific aspects of interest have indeed been outlined by others [8]. These include the potential contrasting effects of precipitated second phases on degrading pure corrosion behaviour and improving erosion resistance compared to single phase CCAs and the need to gain more understanding of aspects of passivation behaviour and synergy mechanisms.

The durability of two laser-clad CCA coatings, $CoCrFeNiMo_{0.85}$ and $Al_{0.5}CoCrFeNi$, were investigated in this work, selected on the basis of their potential to provide good resistance to erosion and corrosion. The detailed rationale for the selection of one coating, $CoCrFeMo_xNi$, has been discussed elsewhere [19] on the basis of its likelihood to provide resistance against wear and corrosion. In particular, recent work has examined the possibility of obtaining high strength from the use of Mo content and appropriate thermal treatments [20]. This provided the intriguing possibility of extending the properties of such HEAs into the realm of wear resistance. The Al-containing CoCrFeNi CCA was selected partly in the light of work [9] on a similar laser-cladded coating which indicated extremely high resistance to cavitation corrosion and improved corrosion resistance versus type UNS S30400 steel in saline solutions. The specific composition selected in this work, $Al_{0.5}CoCrFeNi$, was selected with the aim of obtaining a mixture of both FCC and BCC phases which could provide a ductile (FCC) yet tough (BCC) system.

The present study comprises an assessment of the erosion corrosion performance of two laser clad CCAs ($CoCrFeNiMo_{0.85}$ and $Al_{0.5}CoCrFeNi$) compared to a low-alloy steel (P265GH) and a stainless steel (UNS S30403). Erosion-corrosion testing was conducted with an impinging acidic, saline aqueous solution jet at normal incidence (90°) for 1h. Electrochemical monitoring was conducted in static, flowing and solid-liquid conditions to understand the pure corrosion behaviour of the test materials and its influence on overall damage during erosion corrosion. Post-test metallographic examination was conducted to evaluate the wear mechanisms.

2. Materials and Methods

Two different preparation methodologies were employed for the two CCAs. Gas atomized $CoCrFeNiMo_{0.85}$ powder was produced under argon atmosphere (HERMIGA 75/5 VI EAC, Phoenix Scientific Industries Ltd., Brighton, UK), with an estimated cooling rate of 105–106

°C/s. A powder of final size distribution -48 + 15 μm was finally obtained by means of mechanical sieving. Mechanically alloyed $Al_{0.5}$CoCrFeNi powder were produced from powders of pure elements Co, Cr, Fe, Ni and Mo (Laboratorium®, Bucharest, Romania), processed with a planetary ball mill (Fritsch–Pulverisette 6®, Idar-Oberstein, Germany) for an effective time of 210 min. Elemental powders were placed in a stainless steel vial with stainless steel balls in a 10:1 ball to powder weight ratio for this particular composition. The wet milling process was undertaken, in 2% n-heptane, in order to increase the alloying ratio and decrease the tendency of the powders to adhere onto the balls or vials. From the overall batch of powder produced, a -56 + 20 μm size distribution was extracted by using mechanical sieving. The composition of the materials employed in the work is reported in Table 1 for both CCA coatings and substrates (as provided by the manufacturer). The substrates for the CoCrFeNi$Mo_{0.85}$ and $Al_{0.5}$CoCrFeNi coatings were UNS S30403 and UNS S31600 respectively. The P265GH alloy was included in the test programme to provide information on the behaviour of an alternative, low corrosion resistance, substrate material. Substrates were prepared by mechanical grinding with 60 grit paper followed by acetone degreasing prior to coating deposition.

Mass loss tests were carried out in free erosion-corrosion (FEC) solid-liquid impingement conditions with a recirculating submerged impingement slurry jet test-rig, as illustrated in Figure 1 [21]. The duration of the tests was 1 hour. Slurry impinged at an angle of 90° upon the specimen surface through a nozzle of 4 mm diameter at 18 m/s with a temperature of 40±1 °C. The nozzle was offset from the specimen surface by 5 mm. The slurry consisted of 400 μm angular sand particles with an aqueous solution of pH 4 (obtained by adding HCl) and 3.5% NaCl. The sand concentration was measured to be 0.68 g/l. The test specimens were ground to 1200 grit SiC paper prior to testing. A mass balance with an accuracy of ±0.1 mg was used to measure the mass loss of the test samples. The measured mass losses were converted to volume losses using the nominal densities of the respective test materials. Micro-

hardness profiles of the coatings were measured using a Mitutoyo MVK-G1 micro-hardness testing machine with a 200 gf load.

Potentiodynamic polarisation scans were conducted to assess the electrochemical corrosion rates of the coatings in static, flowing and solid-liquid conditions. The potentiodynamic polarisation scans were conducted at least 15 min after the sample was submerged to allow for the free electrode potential, E_{corr}, to stabilise. A Gill AC potentiostat was utilised for the potentiodynamic polarisation and cathodic protection tests. Platinum was used for the auxiliary electrode and Ag/AgCl employed as the reference electrode. The tests were conducted by shifting the initial potential either 20 mV more positive (cathodic) or 20 mV more negative (anodic) than the free electrode potential, hence ensuring that the transition point would occur. Scans were conducted 300 mV more negative (cathodic) or 300 mV more positive (anodic) at a sweep rate of 15 mV/min. In static conditions, the anodic polarisation curve was pushed positive until the breakdown electrode potential, E_b, was observed. The chosen ranges were sufficient to evaluate corrosion current density measurements by way of the standard electrochemical procedure of Tafel extrapolation. The measured current densities were then used to evaluate the associated volume losses due to corrosion via calculation by Faraday's Law. An electrically conductive wire was connected to the rear of the specimens, which were subsequently cold mounted in epoxy resin. This ensured that only the tested surface was corroding. Impressed current cathodic protection (ICCP) tests were also performed to isolate the pure mechanical damage. In this case, the electrode potential for the CP tests was conducted at -0.8 V (Ag/AgCl) at which potential back extrapolation of the anodic polarisation curves demonstrated that residual anodic reaction rates were negligible.

Microstructural examination of the coatings as well as post-test surface analysis of test specimens was facilitated using a SEM (Hitachi SU-6600) with a 15 kV accelerating voltage. Semi-quantitative EDS analysis was used to evaluate the chemical composition of the coatings. Samples were cross-sectioned, mounted in a conductive resin and polished to 1 μm

SiC. The phase composition of the coatings was studied using X-ray diffraction (XRD) and a Bruker® D8 Advance diffractometer 40 kV, 30 mA, Cu-Kα radiation with λ= 1.5406 Å. Electron Backscattered Diffraction (EBSD) was performed on a Tescan Mira 3 at 30 kV coupled with an Oxford Instruments EBSD detector. The sample was mounted using a 70° pre-tilt stage in the SEM for EBSD scanning. A scanning scheme of 2 × 2 camera binning and 100 nm step size was chosen to capture EBSD patterns.

3. Results and discussion

3.1 Metallurgical examination

Figures 2 and 3 show the microstructural features of the $CoCrFeNiMo_{0.85}$ and $Al_{0.5}CoCrFeNi$ alloys respectively. Both microstructures appeared to have at least two different microstructural phases present. EDS analyses could not conclusively measure any differences in terms of chemical composition for the different microstructural features, hence, XRD was performed – which will be discussed later. The microstructure of $CoCrFeNiMo_{0.85}$, Figure 2 appears to reflect a spinodal decomposition mechanism, which was already reported for the same alloy [22]. An EDS area scan for the $CoCrFeNiMo_{0.85}$, given in Table 3 shows that the composition for the alloy is very similar to the proposed composition – with a slight increase in iron as a result as of some minor dilution effects. Figure 4 displays a cross-sectional image with EDS analysis at different depths of the coating which indicated that the composition was consistent through the coating (Cr – 17 wt.%, Fe – 20-26 wt.%, Co – 15-17 wt.%, Ni – 16-17 wt.%, Mo – 25-29 wt.%). According to the pseudo phase diagram [22] for this composition, spinodal decomposition can be attributed to the spontaneous separation of FCC phase, during alloy solidification, into FCC + σ (and possibly μ although the presence of this phase could not be verified with the analysis techniques employed in this work), driven by the migration of Mo and/or Cr elements. The spinodal decomposition was also observed in the initial powder used to produce this alloy as demonstrated in the SEM and EBSD phase map shown in Figure 5. Figure 5c illustrates two microstructural features; blue coloured FCC phase and a

yellow coloured sigma phase, as identified by the XRD analysis discussed later. Visually, the microstructure of $Al_{0.5}CoCrFeNi$ (Figure 3) appeared to be an equiaxed dendritic structure of a single solid solution phase with a discrete secondary phase of round precipitates located at the intersections of grain boundaries. Some small micro-cracks were also observed, which appear to be localised along grain boundaries. Such cracks in welds or solidified microstructures, such as these obtained by laser cladding, can be classified as either solidification, liquation or ductility-dip cracks, more commonly referred to as hot cracks. EDS analyses was conducted via an area scan (Table 3) as well as spot measurements at different depths of the cross-sectioned coating, as shown in Figure 6. These scans indicated lower than target concentrations of Co (14-18 wt.%), Cr (about 15 wt.%) and Al (3 wt.%) whereas the concentration of iron was measured to be at 36 - 42 wt.% as opposed to 23 wt.% in the theoretical alloy composition. This feature is consistent with weld dilution effects involving convective motion at overlapping passes. EDS analysis was also conducted on the dark spherical phase located in the grain boundaries, however, the analysis was similar to the composition of the main phase due to their small size (approximately 1μm).

Figure 7 shows the X-ray diffraction profiles for the two coatings. In the $CoCrFeNiMo_{0.8}$ coating, a prevalent face-centered-cubic (FCC) crystal structure is identified, together with minor reflections of sigma (σ) phase. The precipitation of hard σ phase, rich in Cr and Mo elements, was observed by Liu et al. [20] on a cast $CoCrFeNiMo_{0.3}$ alloy, while developing high strength high-entropy alloys and this feature appears to be crucially associated with the erosion-corrosion results presented and discussed later in the current paper. It is worth noting that the identification of σ and μ phases, both through XRD analysis is non-trivial as both these phases generally result in several weak peaks in the $\sim35° < 2\theta < \sim50°$ range. The precipitation of σ and μ phases was also observed by Fanicchia et al. [19], in thermally sprayed coatings of the same alloy and by Hong et al., on the same alloy composition [22]. The $Al_{0.5}CoCrFeNi$ coating also appears mainly in the FCC form, with only a small body-

centered cubic (BCC) fraction identified and other smaller diffraction peaks likely related to oxide phases (possibly a combination of Cr_2O_3 and Al_2O_3 [23]). The BCC-stabilising nature of the element Al in alloys of the type $Al_xCoCrFeNi$ has previously been ascertained by several authors. For instance, Wang et al. [24] noted a full FCC crystal structure for $Al_{0-0.4}CoCrFeNi$ alloys, a combined FCC+BCC in $Al_{0.5-0.8}CoCrFeNi$ and a full BCC microstructure for $Al_{>0.8}CoCrFeNi$.

Figure 8 exhibits the measured micro-hardness profiles for both alloys. A minimum of three measurements were collected at each depth; the experimental scatter is shown for each data point. $CoCrFeNiMo_{0.85}$ exhibited the greatest hardness at around 600 HV, which was reasonably consistent throughout the depth of the coating. The micro-hardness, however, tended to vary near the coating-substrate interface, likely due to significant local compositional variations provided by interdiffusion with the substrate. On the other hand, $Al_{0.5}CoCrFeNi$ had a significantly lower micro-hardness (around 180 HV), consistent throughout the depth of the coating and also comparable to the value measured in the substrate.

3.2 Volume loss measurements

Figure 9 shows the free erosion-corrosion (FEC) and cathodic protection (CP) volume losses (calculated from mass loss measurements) results for the tested CCAs. A minimum of two replicates were conducted for each test material/environment. UNS S30403 exhibited the lowest volume loss under FEC conditions, while the $CoCrFeNiMo_{0.85}$ CCA had the lowest volume loss among the CCAs. P265GH steel demonstrated the greatest volume loss in FEC conditions. However, under CP conditions (mechanical damage only), the P265GH steel displayed the lowest volume loss. The $CoCrFeNiMo_{0.85}$ CCA demonstrated the greatest volume loss in CP conditions. Both CCAs and steels exhibited a reduction in volume loss

when CP was applied – which indicates that both are affected - to varying degrees – by corrosion-related mechanisms.

3.3. Potentiodynamic polarisation results

Figures 10-13 show the potentiodynamic polarisation curves for the CCAs and substrate materials under different hydrodynamic conditions (static, flowing and solid-liquid). These results are useful in providing evidence of the CCAs in respect of:

- Resistance to corrosive attack in both static and liquid impingement conditions (i.e. where there is effectively no mechanical wear damage,
- The resistance of the test materials to the onset of localised corrosion,
- For the solid-liquid conditions, enable quantification of the contribution of pure corrosion and the influence of corrosion in enhancing mechanical damage to the overall erosion-corrosion attack on the CCAs.

In Figures 10, 12 and 13, the electrode potential (y-axis) of the potentiodynamic polarisation curves are normalised to the value of E_{corr}, to provide an easier comparison between the different test materials. Note that, in the graphs, an increase in current density corresponds to an increase in corrosion rate. In flowing and solid-liquid conditions, $CoCrFeNiMo_{0.85}$ demonstrates the greatest corrosion resistance due to its potentiodynamic polarisation curve being further to the left compared to the potentiodynamic polarisation curve of the other alloys. The significantly greater resistance to the onset of localised corrosion, of the $CoCrFeNiMo_{0.85}$ alloy, can also be observed in Figure 11, when comparing the breakdown electrode potentials (electrode potential at which the passive oxide film is broken down – indicated by a steep increase in current density).

Table 4 displays the free corrosion electrode potential (E_{corr}), corrosion current densities as well as volume losses due to corrosion for the tested materials in static, liquid only and solid-

liquid conditions. The breakdown electrode potentials, E_b, and the difference between E_b and E_{corr} for the CCAs in static conditions are also given. A more positive value of E_b and a larger value of $E_b - E_{corr}$ are both indicators of higher resistance to the onset of localised corrosion, such as pitting. As quantified in Table 4, in quiescent (static) conditions, the $CoCrFeNiMo_{0.85}$ and UNS S30403 alloys display similar relatively low corrosion rates but, during liquid impingement, the corrosion rates of $CoCrFeNiMo_{0.85}$ are significantly lower compared to $Al_{0.5}CoCrFeNi$ and the steels. The superior corrosion resistance of CoCrFeN-i$Mo_{0.85}$ is further emphasised by its very positive breakdown electrode potential. The good corrosion resistance of $CoCrFeNiMo_{0.85}$ may be related to its relatively high alloying content of Cr, Ni and Mo – all elements which are well-known to boost corrosion resistance of alloys. It is clear, however, that, as argued by Taylor et al. [25], optimising the corrosion resistance with detailed alloy composition in the myriad of CCA compositions requires recourse to fundamental scientific principles. A further complexity is that the corrosion behaviour differences between the two CCAs and the stainless steel become less distinct in the erosion-corrosion (solid-liquid) conditions (Figure 13) because passive films are subject to the periodic breakdown and re-passivation events caused by the impacting sand particles, as shown by the fluctuating currents. Such fluctuating corrosion behaviour is a frequently observed aspect of the corrosion behaviour of passive-film-forming alloys in slurries [21, 26-28].

3.4 Mechanistic breakdown of volume loss

The contribution of the various material degradation mechanisms, associated with erosion-corrosion, to the overall material loss, T, is given in Equation 1.

$$T = M + C + \Delta C_M + \Delta M_C \qquad (1)$$

where pure mechanical damage (M), pure corrosion (C), and the synergy mechanisms of corrosion-enhanced-by-erosion (ΔC_M) and erosion-enhanced-by-corrosion (ΔM_C) have been

specified. The breakdown of degradation mechanisms for the CCAs according to Equation 1 is reported in Figure 14. As demonstrated by the metallurgical examination (section 3.5), the mechanical damage involves erosive attack in the directly impinged zone and abrasive wear in the surrounding regions. The dominant mechanism for the $CoCrFeNiMo_{0.85}$ CCA and the stainless steel was observed to be pure mechanical damage with the pure corrosion and corrosion-enhanced-by-erosion (ΔC_M) terms representing a relatively small proportion of the overall damage. Conversely, for the P265GH carbon steel, the proportion of pure mechanical damage (17%) was less than the contribution (27%) from ΔC_M. The erosion-enhanced-by-corrosion mechanism (ΔM_C) was a particular feature of the damage in carbon steel (52%), $Al_{0.5}CoCrFeNi$ (50%) and was also significant (15%) for $CoCrFeNiMo_{0.85}$.

3.5 Post-test metallurgical examination

Due to the difference in size between the nozzle and test samples, two different hydrodynamic regions occur. Directly below the nozzle, where the wear scar is formed, the sand particles impact the surface at high impingement angles (close to 90° impingement). Whereas, outside the wear scar, the sand particles impact the surface at low impingement angles (close to 5° impingement) which causes sliding abrasion damage on the surface. Post-test microscopy was conducted using SEM. Images were taken both in plan and cross section to review the typical damage mechanisms for the CCAs in these two different hydrodynamic zones. Figure 15 illustrates the damage observed in the wear scar for both CCAs. Small impact craters have been formed caused by the sand particles directly impinging the material surface. This has resulted, where the surface is indented at high impact angles (close to 90° impingement), in plastic deformation damage of the ductile metallic surface with material being smeared to the lip of the impact crater. Repeated impacts have also caused roughening of the ductile surface, due to repeated plastic deformation and smearing. Both wear scars also exhibited some micro-cracking, which can also be observed sub-surface (Figure 16). The cross-sectional images appear to show that the micro-cracks are propagating along the grain boundaries from the

surface, through the coatings before propagating back to the surface – leading to additional material removal.

In the outer area, where the sand particles impact the surface at low angles, sliding abrasion marks are present (Figure 17). This is a result of a cutting-type mechanism on the ductile metallic CCAs which causes the material to plastically deform and smear in the direction of the flow of the impacting particles. It is worth noting that although the degradation rates of the alloys are different (Figures 9 and 14) the degradation mechanisms look similar for both alloys.

4. Detailed discussion

4.1 Corrosion

The evidence from this study indicated that, in quiescent conditions, the $CoCrFeNiMo_{0.85}$ CCA has the twin benefits of extremely low corrosion rates (Figure 10) together with excellent resistance to localised corrosion (Figure 11). Both these characteristics are obviously associated with the spontaneous formation of a protective surface passive film. This feature, together with the considerable superiority over the P265GH alloy, is not unexpected given the overall composition of this CCA alloy with its high Ni, Cr and Mo contents. Although the corrosion rates are similar, the resistance to the onset of localised corrosion of the $CoCrFeNiMo_{0.85}$ CCA is substantially superior to that of the UNS S30403 stainless steel. It should be noted, however, that the high resistance to localised attack – indicated by the large values of E_b and $E_b - E_{corr}$ (Figure 11 and Table 4) - may not be significantly greater than that of higher-grade stainless steels – such as superduplex UNS S32760 – which are well-known to be more resistant to pitting/crevice corrosion than the likes of UNS S30400 or UNS S31600 [29]. A further observed feature that is indicative of superior corrosion resistance of the $CoCrFeNiMo_{0.85}$ CCA over that of UNS S30403 stainless steel, is that the durability of the $CoCrFeNiMo_{0.85}$ CCA is maintained in flowing (non-slurry)

conditions, whereas, the corrosion experienced by the stainless steel increased by about an order of magnitude in flowing – compared to quiescent – conditions.

In contrast, the $Al_{0.5}$CoCrFeNi CCA exhibited considerably higher corrosion susceptibility than either of the other passive alloys in both static and flowing (non-slurry) conditions. This relative vulnerabilty was evident in respect of both measures of corrosion resistance (i_{corr} and $E_b - E_{corr}$). This reduced corrosion resistance may be associated with the presence of the observed precipitate particles (Figures 3 and 16) in compromising corrosion resistance and it is of interest, in this respect, to note that a lower aluminium, $Al_{0.1}$CoCrFeNi CCA (which is said to comprise a single phase FCC structure) has been observed [30] to exhibit substantially higher values of $E_b - E_{corr}$ in NaCl solutions.

The corrosion rates of all the investigated alloys increased when the flowing water contained sand particles. The degrees of enhancement were, however, very different with the $CoCrFeNiMo_{0.85}$ CCA suffering a much greater acceleration of corrosion rate (by approximately 100 times) than the other materials. Indeed this feature resulted in very similar corrosion rates being exhibited by the two CCA alloys and the stainless steel which is indicative that the superior protection afforded by the passive film on the $CoCrFeNiMo_{0.85}$ CCA in the two less-aggressive environmental conditions is not maintained under the extreme circumstances provoked by the impacting sand particles.

4.2 Influence of corrosion on erosion-corrosion performance

This factor can have a profound influence – especially in relation to materials of low inherent corrosion resistance such as carbon steel. Indeed, when the corrosion factor is eliminated by the application of cathodic protection, it is evident that the higher grades of metallic alloys, such as $CoCrFeNiMo_{0.85}$ CCA and stainless steels, offer less benefit in terms of pure mechanical damage than carbon steel and low-alloy steels [27, 31, 32]. This is a potentially

useful feature that, as has been argued by the authors, [32, 33], is perhaps worthy of consideration at least for some industrial situations.

The contribution of corrosion to the overall damage of the P265GH carbon steel involved pure corrosion and both the synergy mechanisms. In respect of the other three, more corrosion resistant, alloys, however, it is interesting to note that the influence of corrosion is not particularly related to pure electrochemical attack (parameter "C" in equation 1 above) or, indeed to turbulence in raising corrosion rates (ΔC_M) but is often more substantive in terms of the other synergy component (ΔMc) which is a measure of the role of corrosion in elevating the amount of mechanical damage. This factor is a particular feature of the behaviour of the $Al_{0.5}CoCrFeNi$ CCA (Figure 14) and likely mechanisms are discussed below. The role of this synergy factor has been missed in some related work [18].

The damage associated with the erosion-enhanced-by-corrosion (ΔM_c) mechanism is likely to involve galvanic interactions between the different microstructural features observed in both CCAs. Such electrically connected microstructural phases, with different electrode potentials, have been reported to lead to micro-galvanic corrosion between the phases [34, 35]. The resulting weakened interface will clearly lead to accelerated dislodgement of material under the action of the impacting solid particles. This form of ΔM_c occurs to a variable extent in the different alloys because its severity is dependent upon the actual dispersion and composition of the phases. For instance, the severity has been proven small in the UNS S30403 steel, presumably on account of the single phase (austenitic) microstructure of this alloy. The cause of the ΔM_C mechanism for UNS S30403 (which contributed to 13% of the overall damage) is, as suggested by Matsumura et al. [36] more likely to involve corrosion removing the work hardened layer which in turn causes the stainless steel to be more susceptible to mechanical damage. For carbon steels, the ΔM_C mechanism (amounting to 52% of the overall erosion-corrosion damage) can be attributed to the formation of corrosion pits. These cause local turbulence which in turn enhances mechanical erosion damage. Additionally, corrosion has

been observed to roughen the surface by the formation of micro-turbulence, effect that would be exacerbated by corrosion pits [37].

4.3 Overall erosion-corrosion behaviour

A material with optimum resistance to erosion-corrosion must possess good resistance to mechanical and corrosion damage. The $CoCrFeNiMo_{0.85}$ CCA exhibited rather better resistance to solid-liquid conditions than the other CCA. This may be associated with the following features:

- A smaller contribution from corrosion to the overall damage, as evident in Figure 14.
- The constitution of the $CoCrFeNiMo_{0.85}$ CCA conferring improvements in resistance to applied stresses involving the role of the intermetallic compounds such as σ and μ, as well as possibly the intrinsic spinodal decomposition microstructure of FCC matrix. For example, the precipitation of hard σ phase, rich in Cr and Mo, was observed by Liu et al., [20], on a cast $CoCrFeNiMo_{0.3}$ alloy, while developing high strength high-entropy alloys. In the study, the segregation of both σ and μ intermetallics in the FCC matrix led to a ~40% increment in Ultimate Tensile Strength (UTS) compared to a pure FCC as-cast $CoCrFeNiMo_{0.3}$ alloy. The observation, in the current study, of the presence of σ phase in the $CoCrFeNiMo_{0.85}$ coating presents persuasive evidence for its influence on the hardness of this CCA. Of course, the presence of such precipitate particles in conventional stainless steels is well established but an often-found issue with the presence of such intermetallics is their potential deleterious influence on both mechanical strength and corrosion resistance [38]. In this work, however, both the corrosive wear resistance and the corrosion resistance have been found to be very satisfactory.

However, whether such improvements in strength and hardness translate into resistance to erosion is not absolutely clear. Fracture toughness may be a more relevant parameter to correlate wear with conventional mechanical properties [39, 40]. It would be expected that

any such hardness/strength factors would be evident in terms of resistance to pure mechanical damage but Figure 9 does not support this notion in relation to the specific CCAs and conditions investigated in this study. A more persuasive explanation of the erosion-corrosion results may therefore be based on the influence of corrosion (first bullet point above). Indeed, the relative performances of the two CCAs is clearly related to their different vulnerabilities to corrosion. The inferior corrosion behaviour of the $Al_{0.5}$CoCrFeNi CCA is likely to be associated with the presence of intermetallic phases facilitating micro-galvanic action at grain boundary locations. This feature would account for the high ΔMc contribution to the overall damage in this material. The CP results (Figure 9) indicate that the $Al_{0.5}$CoCrFeNi CCA possesses better resistance to pure mechanical damage than the other CCA. This is despite the considerably lower hardness of the $Al_{0.5}$CoCrFeNi CCA and perhaps implies that different types of CCA may be appropriate for low-angle impingement – which is akin to abrasive flow and where high strength/hardness might be optimum – as opposed to high angle attack where classical erosion theory [41] states that brittle cracking type damage does not favour high strength materials.

It is also of interest to assess any benefits of CCAs in comparison with the conventional competitive materials such as carbon steels and stainless steels. This study and others [17] have established the superiority of various CCAs over carbon steels and, thereby, signalled a potential benefit for coating carbon steel with an appropriate CCA. Clearly, though, the poor corrosion resistance of carbon steel places a premium on the protective efficiency of any coating. In particular reference to the materials studied in this research, it is noteworthy that Fanicchia et al. [19] demonstrated this aspect of the vulnerability of carbon steel, when HVOF-coated with $CoCrFeNiMo_{0.85}$ CCA, resulting from permeation of corrosive liquid through the coating thickness to the carbon steel substrate.

This study, however, has not unearthed any such beneficial effects when comparing the CCAs with UNS S30403 and the evidence from other works [8-10, 17] throw up rather varying

evidences. The relative performances of CCAs and stainless steels may, as observed in one study [18], be impingement-angle dependent. Appropriate CCAs benefit by the greater vulnerability to mechanical damage at intermediate angles but are less competitive at 90° impingement – where a high strength CCA might be more vulnerable to brittle mechanisms of erosion [41]. Such an argument, however, ignores the crucial role of corrosive attack at different angles but might support the notion of a relatively large role of abrasive mechanical damage at low angles on account of the considerably lower corrosion rates at glancing angles.

5. Conclusions

This study has focused on LMD coatings $CoCrFeNiMo_{0.85}$ and $Al_{0.5}CoCrFeNi$, produced by two, well-known CCAs that have been formulated to comprise largely FCC structures but also containing arrays of second-phase phases/precipitates. The corrosion and erosion-corrosion behaviour of these two CCAs has been compared to two common steels: austenitic stainless steel - UNS S30403 and P265GH. Below are the main findings from this study.

- In quiescent and flowing (non-slurry) solutions, the $CoCrFeNiMo_{0.85}$ alloy was the most corrosion resistant material in this study – with the lowest overall corrosion rate and considerably higher resistance to the onset of localised corrosion. This excellent durability is likely to be associated with the high molybdenum content, despite the presence of sigma phase which is generally found to increase corrosion susceptibility in stainless steel alloys.

- In slurry conditions, all passive alloys demonstrated similar pure corrosion and erosion-corrosion rates. On all these materials, the common feature was of repetitive de-passivation/re-passivation behaviour.

- In all materials, - although to a varied extent – the corrosion-related attack represented a significant contribution to the overall material losses. The carbon steel was observed to be particularly vulnerable to this type of attack. For all alloys, the most prevalent corrosion-related attack was erosion enhanced by corrosion.

- The observed relatively high rate of corrosion-enhanced mechanical damage for the $Al_{0.5}CoCrFeNi$ alloy appears to be associated with micro-galvanic interactions involving the array of particles present at grain boundaries.

- The mechanisms of erosion-corrosion were similar for the two HEA alloys – comprising abrasion corrosion in the outer regions as well as plastic deformation and micro-cracking at perpendicular impingement.

Acknowledgements

The authors would also like to acknowledge the resources and collaborative efforts provided by the University Politehnica of Bucharest and the whole consortium of the Geo-Coat project. As well as, the support provided by the Weir Group PLC (WARC2011-SAA1, 2011) via its establishment of the Weir Advanced Research Centre (WARC) at the University of Strathclyde.

Funding

This work is part of the H2020 EU project Geo-Coat: "Development of novel and cost-effective corrosion resistant coatings for high temperature geothermal applications" funded by the H2020 EU project no. 764086.

References

[1] J.-W. Yeh, S.-K. Chen, S.-J. Lin, J.-Y. Gan, T.-S. Chin, T.-T. Shun, C.-H. Tsau, S.-Y. Chang, Nanostructured High-Entropy Alloys with Multiple Principal Elements: Novel Alloy Design Concepts and Outcomes, Adv. Eng. Mats. 5 (2004) 299-303. https://doi.org/10.1002/adem.200300567

[2] Y. F. Ye, Q. Wang, J. Lu, C. T. Liu, Y. Yang, High-entropy alloy: challenges and prospects. Materials Today 19 (2016) 349-362. https://doi.org/10.1016/j.mattod.2015.11.026

[3] D. B. Miracle, O. N. Senkov, A critical review of high entropy alloys and related concepts. Acta Materialia 122 (2017) 448-511. https://doi.org/10.1016/j.actamat.2016.08.081

[4] A. D. Pogrebnjak, A. A. Bagdasaryan, I. V. Yakushchenko, V. M. Beresnev, The structure and properties of high-entropy alloys and nitride coatings based on them, Russian Chemical Reviews 83:11 (2014) 1027 – 1061. https://doi.org/10.1070/RCR4407

[5] S. S. Nene, S. Sinha, M. Frank, K. Liu, R. S. Mishra, B. A. McWilliams, K. C. Cho, Unexpected strength-ductility response in an annealed, metastable, high-entropy alloy. Applied Materials Today 13 (2018) 198-206. https://doi.org/10.1016/j.apmt.2018.09.002

[6] V. Buranich, V. Rogoz, B. Postolnyi, A. Pogrebnjak, Predicting the Properties of the Refractory High-Entropy Alloys for Additive Manufacturing-Based Fabrication and Mechatronic Applications, 2020 IEEE 10th International Conference Nanomaterials: Applications & Properties (NAP). https://doi.org/10.1109/NAP51477.2020.9309720

[7] A. D. Pogrebnjak , I. V. Yakushchenko , A. A. Bagdasaryan , O. V. Bondar , R. Krause-Rehberg, G. Abadias, P. Chartier, K. Oyoshi, Y. Takeda, V. M. Beresnev, O. V. Sobol, Microstructure, physical and chemical properties of nanostructured (TiHfZrVNb)N coatings under different deposition conditions, Materials Chemistry and Physics, 147 (2014) 1079-1091. https://doi.org/10.1016/j.matchemphys.2014.06.062

[8] A. Ayyagari, V. Hasannaeimi, H. S. Grewal, H. Arora, S. Mukherjee, Corrosion, erosion and wear behavior of complex concentrated alloys: A review. Metals 8:8 (2018) 603. https://doi.org/10.3390/met8080603

[9] S. Zhang, C. L. Wu, C. H. Zhang, M. Guan, J. Z. Tan, Laser surface alloying of FeCoCrAlNi high-entropy alloy on 304 stainless steel to enhance corrosion and cavitation erosion resistance. Optics & Laser Technology 84 (2016) 23-31. https://doi.org/10.1016/j.optlastec.2016.04.011

[10] J. Zhao, A. Ma, X. Ji, J. Jiang, Y. Bao, Slurry erosion behavior of AlxCoCrFeNiTi0.5 high entropy alloy coatings fabricated by laser cladding. Metals 8 (2018) 126. https://doi.org/10.3390/met8020126

[11] Y. Shi, B. Yang, P. K. Liaw, Corrosion-resistant high-entropy alloys: a review. Metals 7:2 (2017) 43. https://doi.org/10.3390/met7020043

[12] R. B. Nair, H. S. Arora, S. Mukherjee, S. Singh, H. Singh, H. S. Grewal, Exceptionally high cavitation erosion and corrosion resistance of a high entropy alloy. Ultrason Sonochem. 41 (2018) 252-260. https://doi.org/10.1016/j.ultsonch.2017.09.044

[13] Q. Ye, K. Feng, Z. Li, F. Lu, R. Li, J. Huang, Y. Wu, Microstructure and corrosion properties of CrMnFeCoNi high entropy alloy coating. Applied surface science 396 (2017) 1420-1426. https://doi.org/10.1016/j.apsusc.2016.11.176

[14] Y. Qiu, M. A. Gibson, H. L. Fraser, N. Birbilis, Corrosion characteristics of high entropy alloys. Materials Science & Technology 31:10 (2015) 1235-1243. https://doi.org/10.1179/1743284715Y.0000000026

[15] E. P. George, W. A. Curtin, C. C. Tasan, High entropy alloys: A focused review of mechanical properties and deformation mechanisms. Acta Materialia 188 (2020) 435-474. https://doi.org/10.1016/j.actamat.2019.12.015

[16] C. L. Wu, S. Zhang, C. H. Zhang, H. Zhang, S. Y. Dong, Phase evolution and cavitation erosion-corrosion behavior of FeCoCeAlNiTix high entropy alloy coatings on 304 stainless steel by laser surface alloying. Journal of Alloys and Compounds 698 (2017) 761-770. https://doi.org/10.1016/j.jallcom.2016.12.196

[17] R. B. Nair, K. Selvam, H. S. Arora, S. Mukherjee, H. Singh, H. S. Grewal, Slurry erosion behavior of high entropy alloys. Wear 386-387 (2017) 230-238. https://doi.org/10.1016/j.wear.2017.01.020

[18] R. B. Nair, H. S. Arora, A. Ayyagari, S. Mukherjee, H. S. Grewal, High entropy alloys: Prospective materials for tribo-corrosion applications. Advanced Engineering Materials 20:6 (2018) 1700946. https://doi.org/10.1002/adem.201700946

[19] F. Fanicchia, I. Csaki, L. E. Geambazu, H. Begg, S. Paul, Effect of microstructural modifications on the corrosion resistance of CoCrFeMo0.85Ni compositionally complex alloy coatings. Coatings 9:11 (2019) 695. https://doi.org/10.3390/coatings9110695

[20] W. H. Liu, Z. P. Lu, J. H. Luan, Z. J. Wang, B. Liu, Y. Liu, M. W. Chen, C. T. Liu, Ductile CoCrFeNiMox high entropy alloys strengthened by hard intermetallic phases. Acta Materialia 116 (2016) 332-342. https://doi.org/10.1016/j.actamat.2016.06.063

[21] F. Brownlie, C. Anene, T. Hodgkiess, A. Pearson, A. M. Galloway, Comparison of Hot Wire TIG Stellite 6 weld cladding and lost wax cast Stellite 6 under corrosive wear conditions. Wear 404-405 (2018) 71-81. https://doi.org/10.1016/j.wear.2018.03.004

[22] Z. Dong, D. Sergeev, M. F. Dodge, F. Fanicchia, M. Müller, S. Paul, H. Dong, Microstructure and Thermal Analysis of Metastable Intermetallic Phases in High-Entropy Alloy CoCrFeMo0.85Ni. Materials 14 (2021) 1073. https://doi.org/10.3390/ma14051073

[23] A. Mohanty, J. K. Sampreeth, O. Bembalge, J. Y. Hascoet, S. Marya, R. J. Immanuel, S. K. Panigrahi, High temperature oxidation study of direct laser deposited AlxCoCrFeNi (x=0.3,0.7) high entropy alloys. Surface and coatings technology 380 (2019) 125028. https://doi.org/10.1016/j.surfcoat.2019.125028

[24] W.-R. Wang, W.-L. Wang, S.-C. Wang, C.-H. Lai, J. W. Yeh, Effects of Al addition on the microstructure and mechanical property of AlxCoCrFeNi high-entropy alloys. Intermetallics 26 (2012) 44-51. https://doi.org/10.1016/j.intermet.2012.03.005

[25] C. D. Taylor, P. Lu, J. Saal, G. S. Frankel, J. R. Scully, Integrated computational materials engineering of corrosion resistant alloys. Npj Materials Degradation 2:6 (2018). https://doi.org/10.1038/s41529-018-0027-4

[26] G. Karafyllias, A. M. Galloway, E. Humphries, The effect of low pH in erosion-corrosion resistance of high chromium cast irons and stainless steels. Wear 37:8 (2018) 79-86. https://doi.org/10.1016/j.wear.2018.11.021

[27] L. Giourntas, T. Hodgkiess, A. M. Galloway, Enhanced approach of assessing the corrosive wear of engineering materials under impingement. Wear 338-339 (2018) 155-163. https://doi.org/10.1016/j.wear.2015.06.004

[28] S. Aribo, R. Barker, X. Hu, A. Neville, Erosion-corrosion behavior of lean duplex stainless steels in 3.5% NaCl solution. Wear 302 (2013) 1602-1608. https://doi.org/10.1016/j.wear.2012.12.007

[29] H.-Y. Ha, T.-H. Lee, J.-H Bae, D. W. Chun, Molybdenum effects on pitting corrosion resistance of FeCrMnMoNC austenitic stainless steels. Metals 8:8 (2018) 653. https://doi.org/10.3390/met8080653

[30] K. Wang, D. Lan, J. W. Qiao, Corrosion behavior of Al0.1CoCrFeNi High Entropy Alloy in Various Chloride-Containing Solutions. Front. Mater. 7 (2021) 533843. https://doi.org/10.3389/fmats.2020.533843

[31] F. Smith, F. Brownlie. T. Hodgkiess, A. Toumpis, A. Pearson, A. M. Galloway, Effect of salinity on the corrosive wear behaviour of engineering steels in aqueous solutions. Wear, 462-463 (2020) 203515. https://doi.org/10.1016/j.wear.2020.203515

[32] F. Brownlie, T. Hodgkiess, A. Pearson, A. M. Galloway, A study on the erosion-corrosion behaviour of engineering materials used in the geothermal industry. Wear, 2021, 203821. https://doi.org/10.1016/j.wear.2021.203821

[33] F. Brownlie, L. Giourntas, T. Hodgkiess, I. Palmeira, O. Odutayo, A. M. Galloway, A. Pearson, Effect of cathodic protection methods on ferrous engineering materials under corrosive wear conditions. Corrosion Engineering, Science and Technology 55:6 (2020) 480-486. https://doi.org/10.1080/1478422X.2020.1742997

[34] J.-S. Lee, K. Fushimi, T. Nakanishi, Y. Hasegawa, Y.-S. Park, Corrosion behavior of ferrite and austenite phases on super duplex stainless steel in a modified green-death solution. Corrosion Science 89 (2014) 111-117. https://doi.org/10.1016/j.corsci.2014.08.014

[35] Y. H. Yau, M. A. Streicher, Galvanic corrosion of duplex FeCr-10%Ni alloys in reducing acids. Corrosion 43:6 (1987) 366-373. https://doi.org/10.5006/1.3583872

[36] M. Matsumura, Erosion-corrosion: An Introduction to Flow Induced Macro-Cell Corrosion, 2nd ed.; Bentham Science Publishers: Sharjah, UAE, 2012.

[37] T. J. Harvey, J.A. Wharton, R. J. K. Wood, Development of synergy model for erosion-corrosion of carbon steel in a slurry pot. Tribology 1:1 (2007) 33-47. https://doi.org/10.1179/175158407X181471

[38] W. Yongqiang, S. Hao, L. Na, X. Yanhao, J. Hemin, Effect of sigma phase precipitation on the pitting corrosion mechanism of duplex stainless steels. International Journal of Electrochemical Science 13 (2018) 9868-9887. https://doi.org/10.20964/2018.10.38

[39] A. R. Chintha, K. Valtonen, V.-T. Kuokkala, S. Kundu, M. J. Peet, H. K. D. H. Bhadeshia, Role of fracture toughness in impact-abrasion wear. Wear 428-429 (2019) 430-437. https://doi.org/10.1016/j.wear.2019.03.028

[40] F. Brownlie, T. Hodgkiess, A. M. Galloway, A. Pearson, Experimental investigation of engineering materials under repetitive impact slurry conditions. Tribology Letters 69:5 (2021) 311. https://doi.org/10.1007/s11249-020-01381-y

[41] I. M. Hutchings, Ductile-brittle transitions and wear maps for the erosion and abrasion of brittle materials. Journal of Physics D: Applied Physics, 1991, 212, 212-221. https://doi.org/10.1088/0022-3727/25/1A/033

Table 1: Nominal chemical composition (wt.%) of CCA coatings and substrates

Element (wt.%)	Co	Cr	Fe	Ni	Mo	Al	C	Mn	Si
$CoCrFeNiMo_{0.85}$	19.2	16.9	18.9	19.1	26.6	-	-	-	-
$Al_{0.5}CoCrFeNi$	24.7	21.8	23.4	24.6		5.6			
UNS S30403	-	18-20	Bal.	8-12	-	-	0.035 max.	2 max.	1 max.
UNS S31600	-	16-18	Bal.	10-14	2-3	-	0.08 max.	2 max.	0.75 max.
P265GH	-	0.3	Bal.	0.3	0.08	0.02	0.2	0.6-1.2	0.35

Table 2: LMD parameters used to produce CCAs

Alloy	Laser power (W)	Laser speed (mm/s)	Powder disc speed (%)	Carrier gas (L/min)
$CoCrFeNiMo_{0.85}$	550	10	9.3	3.5
$Al_{0.5}CoCrFeNi$	550	10	8.7	4

Table 3: EDS area scan analysis (wt.%) for both CCAs and their proposed composition (wt.%)

Analysis	Al	Si	Cr	Fe	Co	Ni	Mo
				$CoCrFeNiMo_{0.85}$			
Measured	-	-	17	24	16	17	27
Proposed	-	-	16.9	18.9	19.2	19.1	26.6
				$Al_{0.5}CoCrFeNi$			
Measured	3	0.3	15	41	15	26	-
Proposed	5.6	-	21.8	23.4	24.7	24.6	-

Table 4: Free corrosion electrode potential (E_{corr}), corrosion current density (i_{corr}) and volume loss due to corrosion for the CCAs and steels in static, flowing and solid-liquid conditions. Breakdown potentials (E_b) also stated for the CCAs and stainless steel in static conditions.

	CoCrFeNiMo$_{0.85}$	**Al$_{0.5}$CoCrFeNi**	**UNS S30403**	**P265GH**
Static				
E_{corr} (mV)	-168	-388	-159	-565
E_b (mV)	1004	-311	52	-
$E_b - E_{corr}$ (mV)	1172	77	211	-
i_{corr} (mA/cm^2)	0.0001	0.0055	0.0002	0.07
Volume loss due to corrosion (mm^3/hr)	0.00007	0.004	0.0003	0.15
Flowing				
E_{corr} (mV)	1	-367	-76	-468
i_{corr} (mA/cm^2)	0.00013	0.0045	0.002	0.4
Solid-liquid				
E_{corr} (mV)	-385	-395	-464	-494
i_{corr} (mA/cm^2)	0.01	0.015	0.023	0.55
Volume loss due to corrosion (mm^3/hr)	0.006	0.0097	0.033	1.28

List of Figures

Figure 15: Plan view of damage in wear scar for $CoCrFeNiMo_{0.85}$ (A) and $Al_{0.5}CoCrFeNi$ (B), corresponding to high angle impact

Figure 16: Cross section view of damage in wear scar for $CoCrFeNiMo_{0.85}$ (A) and $Al_{0.5}CoCrFeNi$ (B)

Figure 17: Plan view of damage in outer area for $CoCrFeNiMo_{0.85}$ (A) and $Al_{0.5}CoCrFeNi$ (B), corresponding to low-angle impact

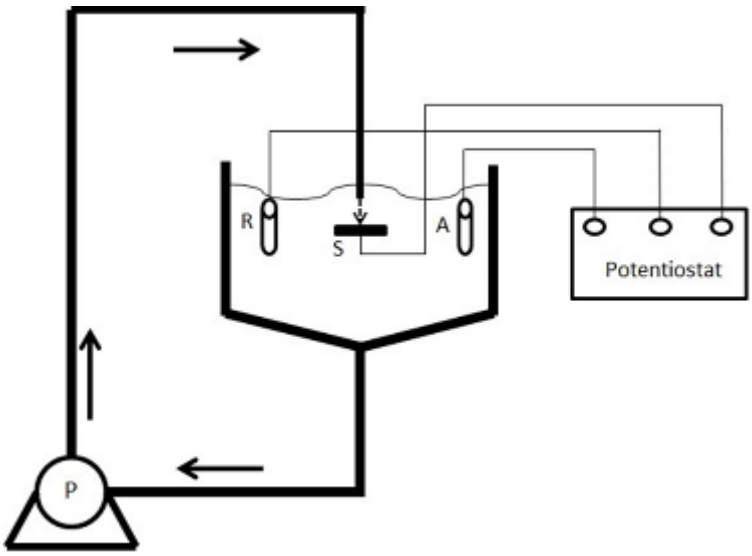

Figure 1

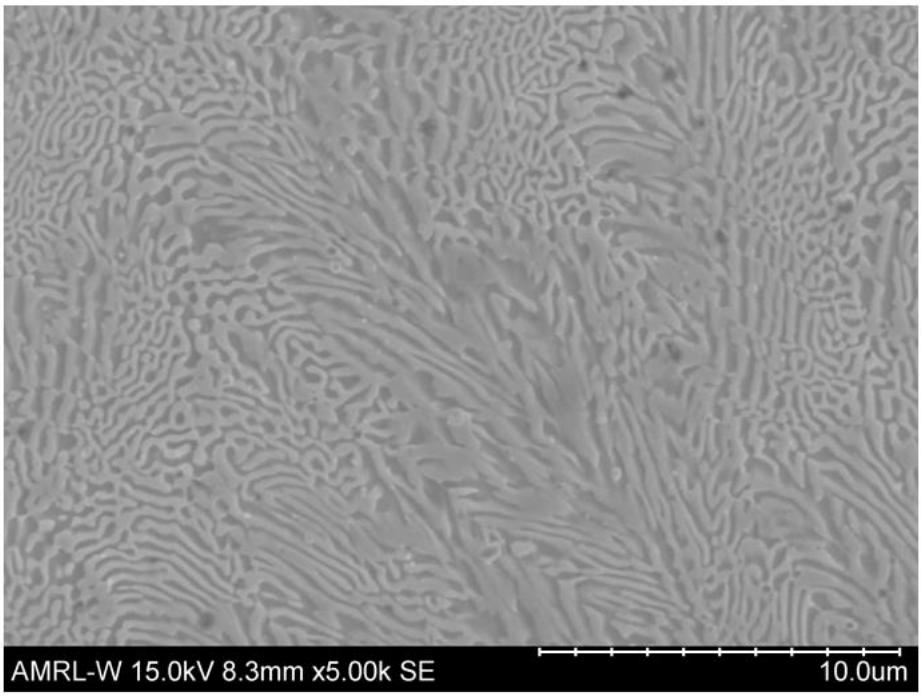

Figure 2

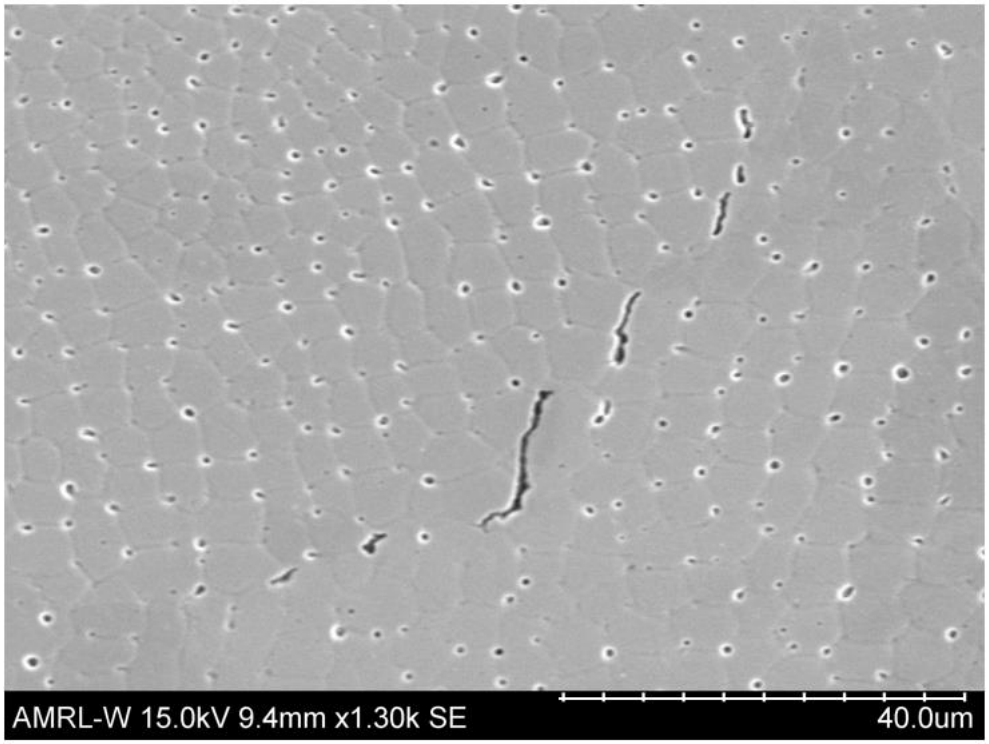

Figure 3

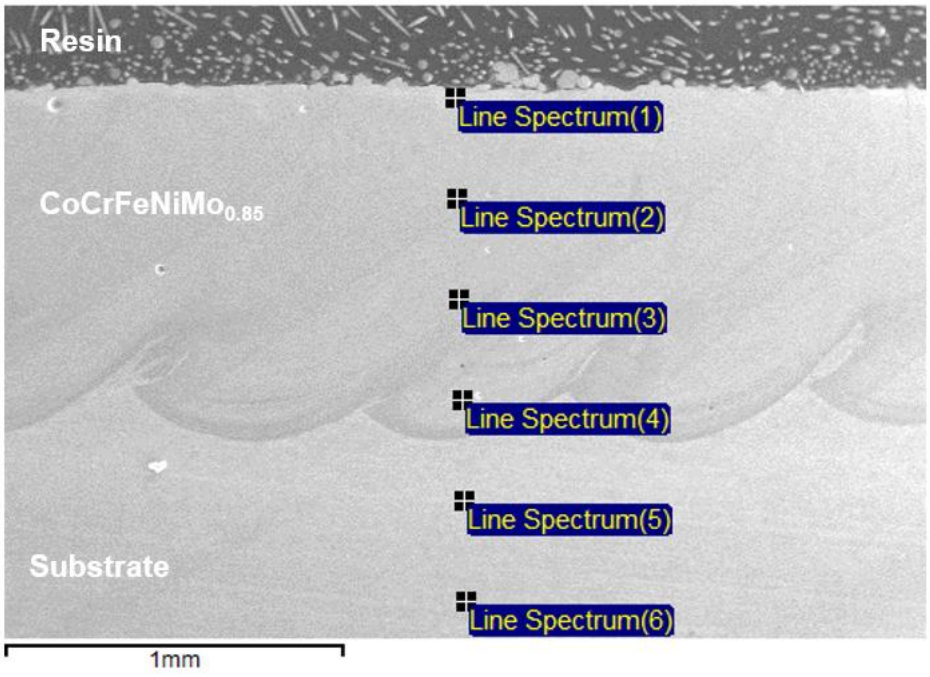

Figure 4

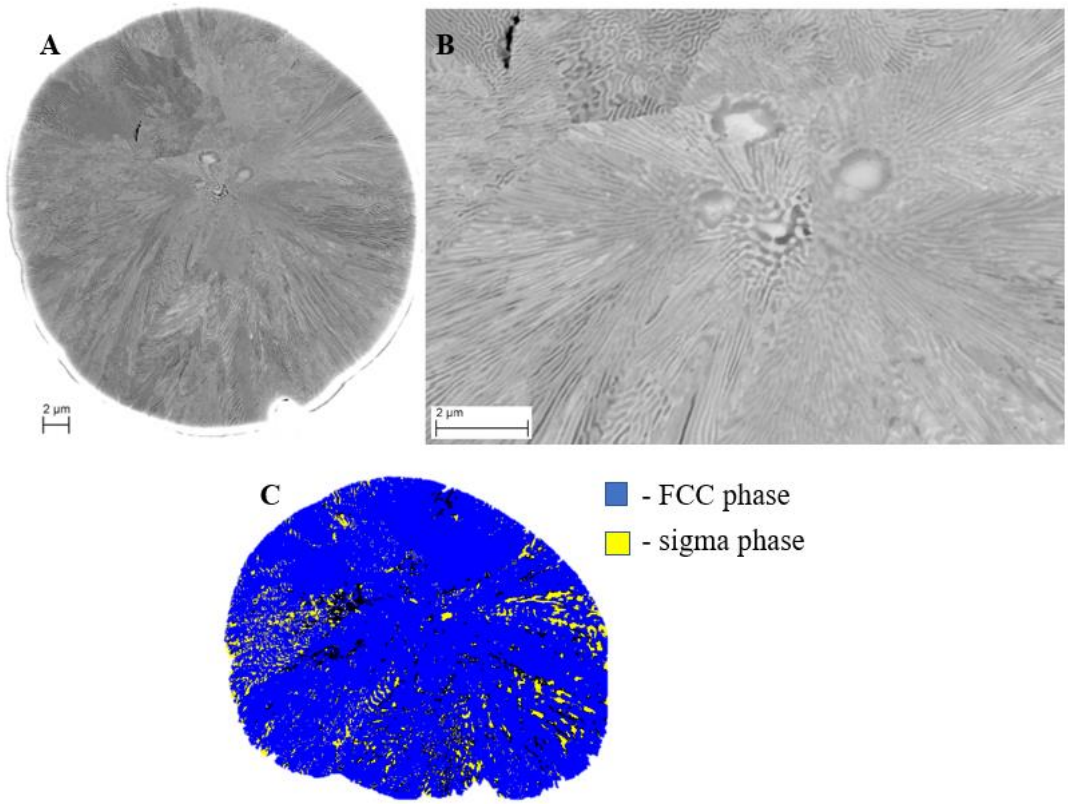

Figure 5

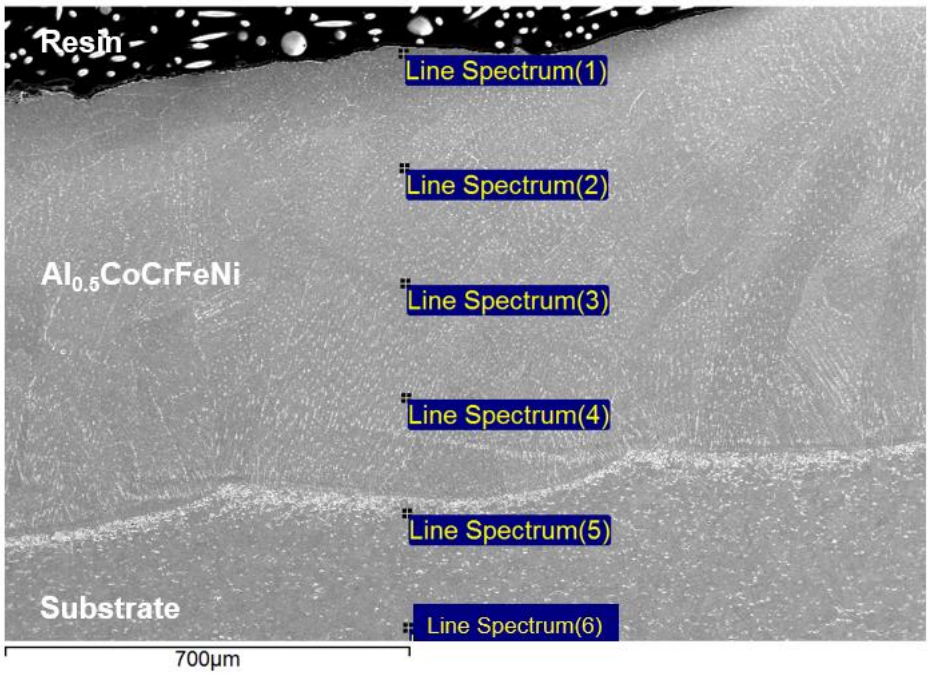

Figure 6

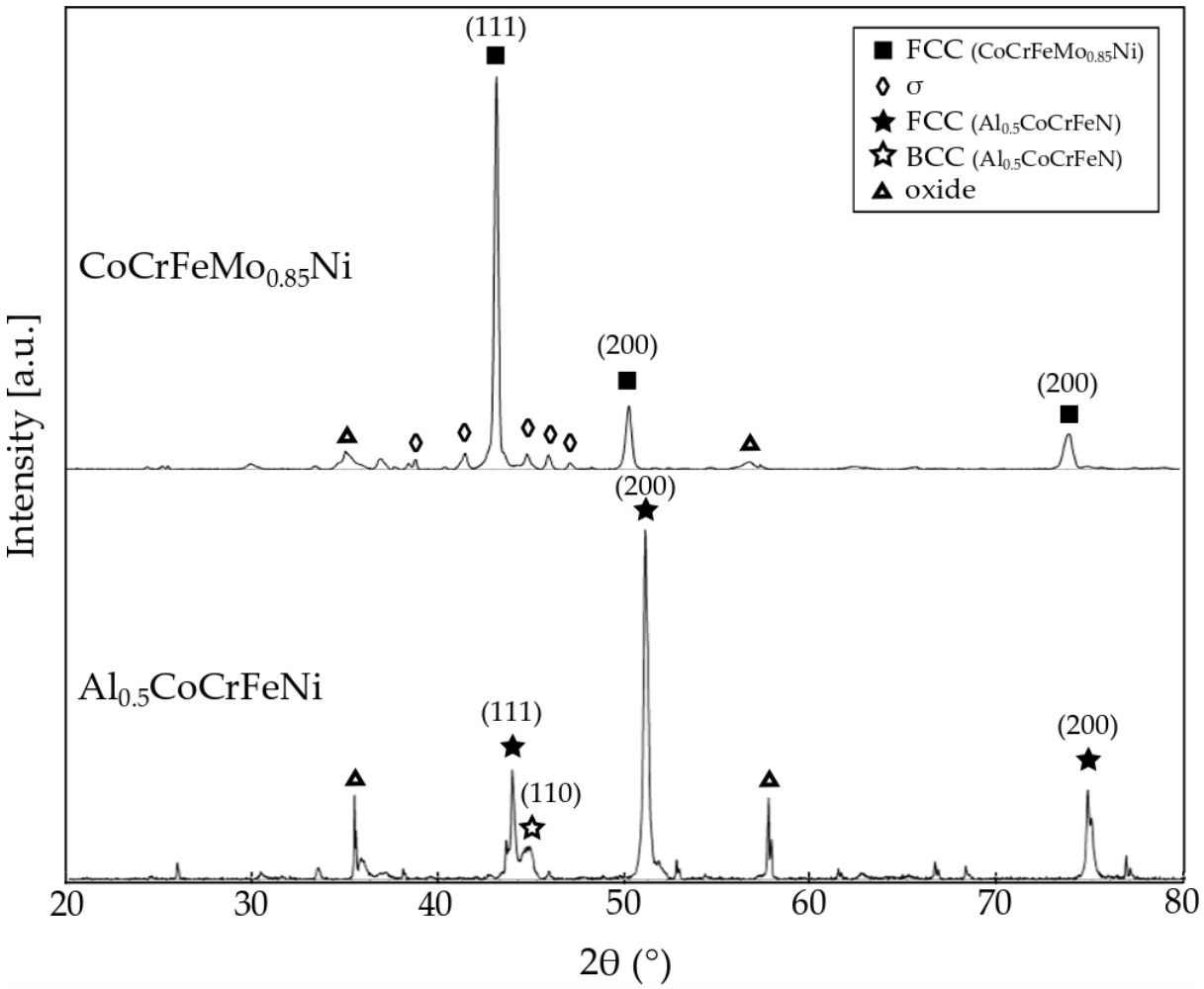

Figure 7

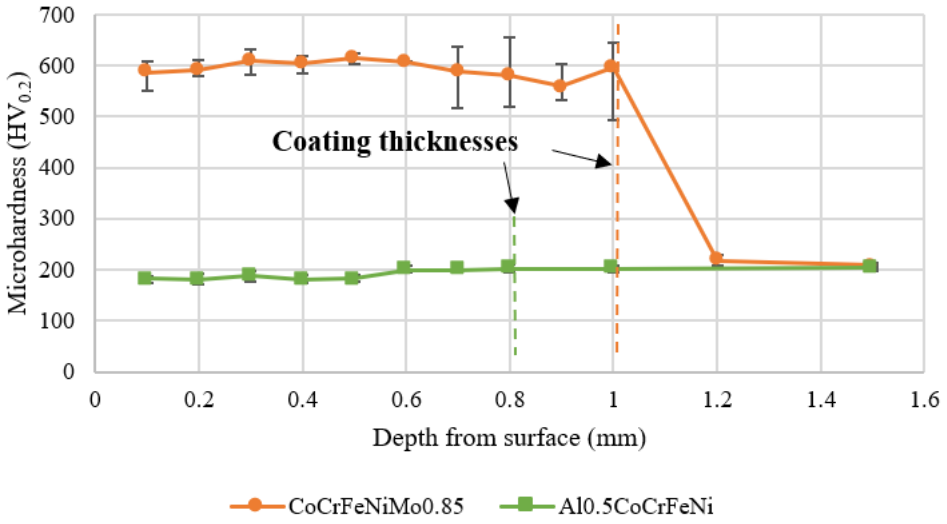

Figure 8

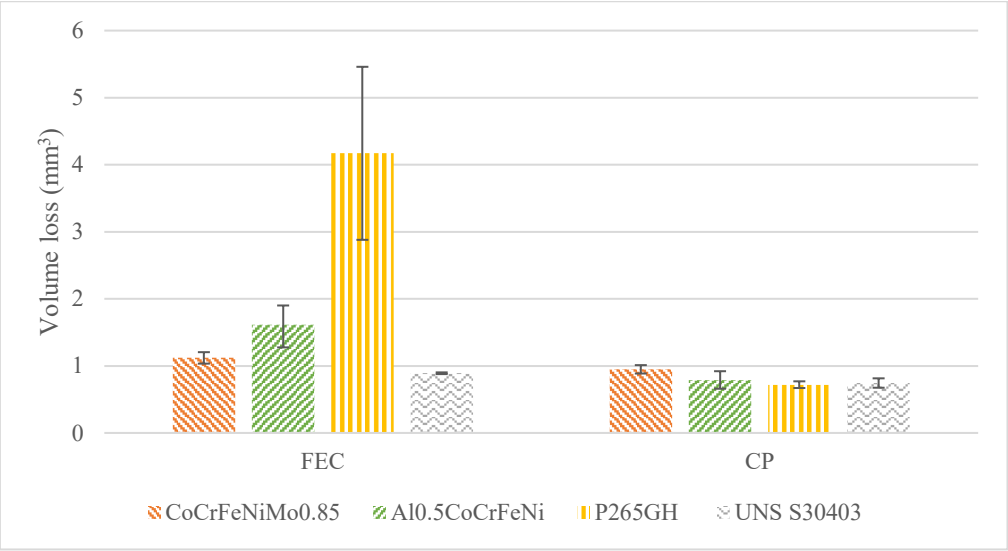

Figure 9

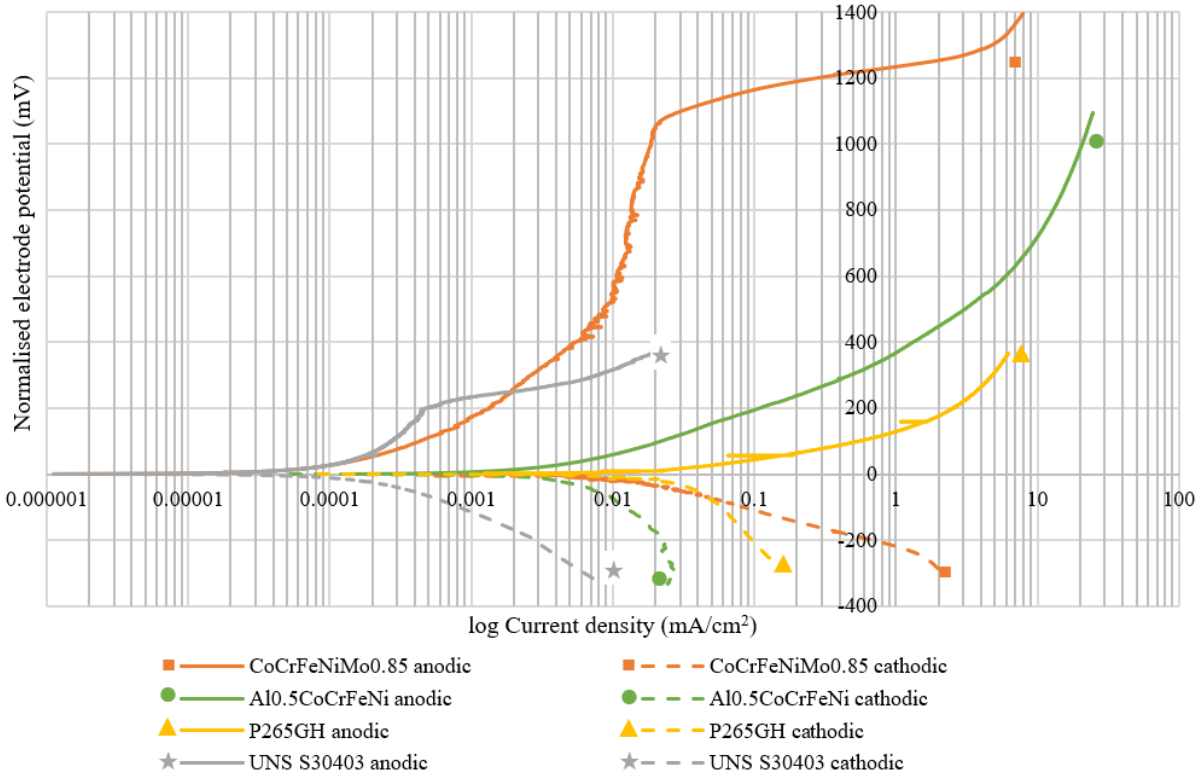

Figure 10

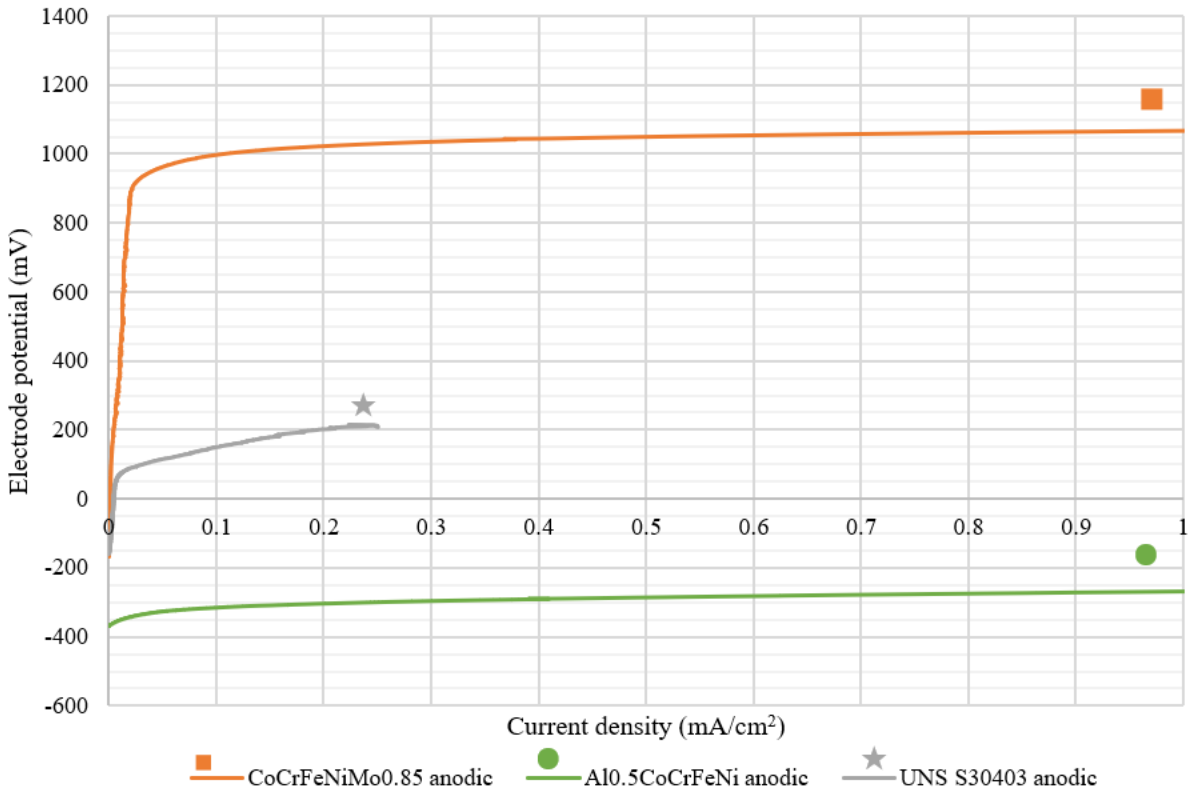

Figure 11

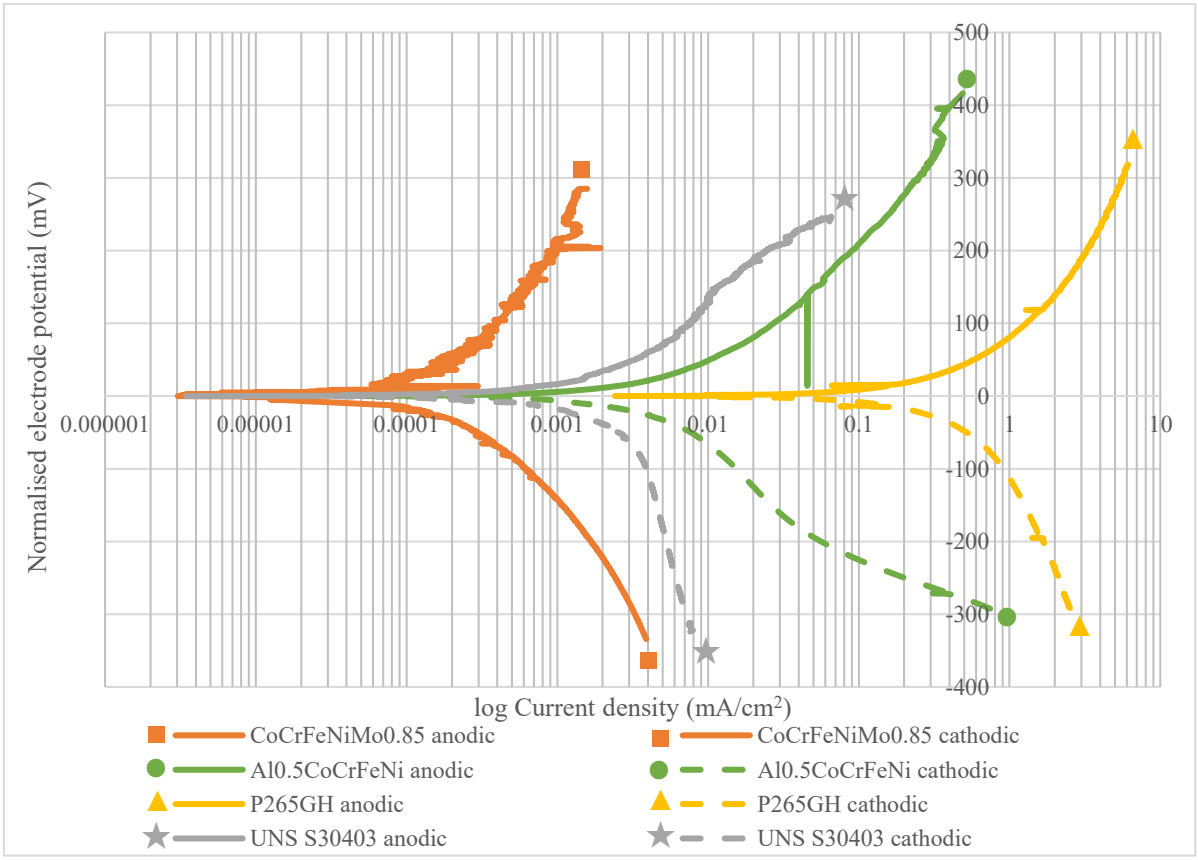

Figure 12

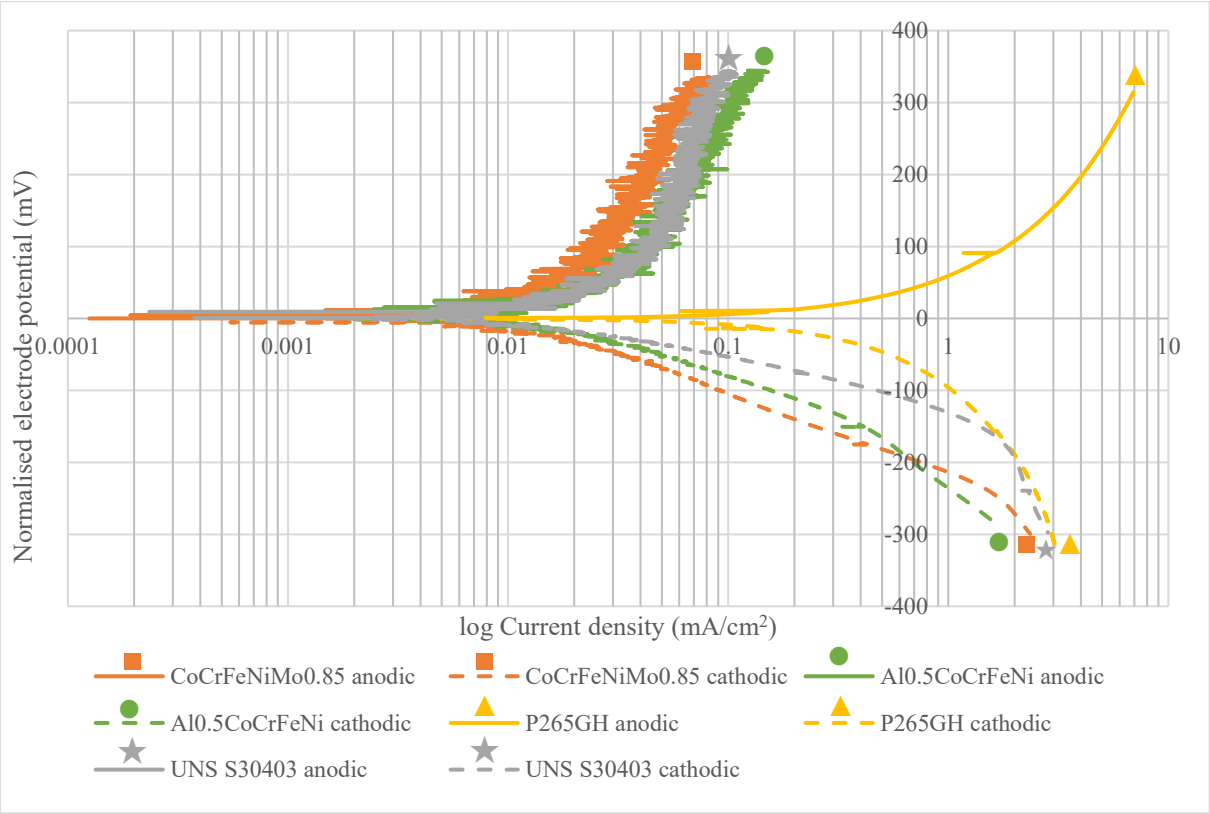

Figure 13

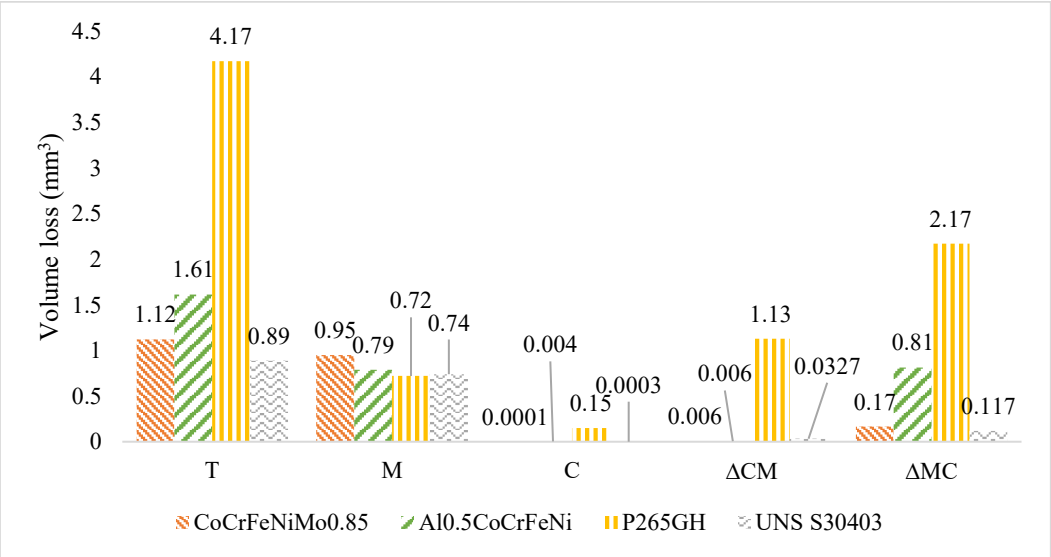

Figure 14

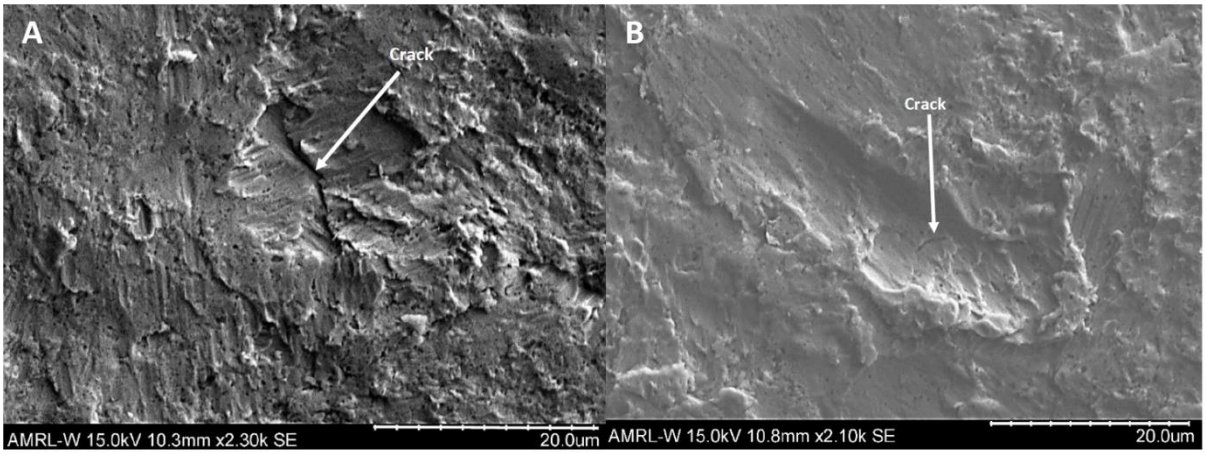

Figure 15

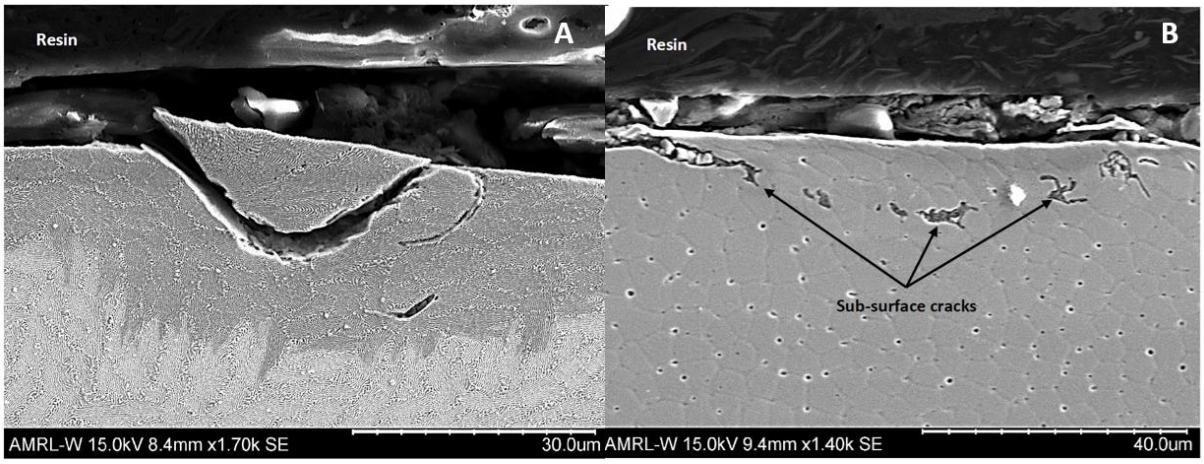

Figure 16

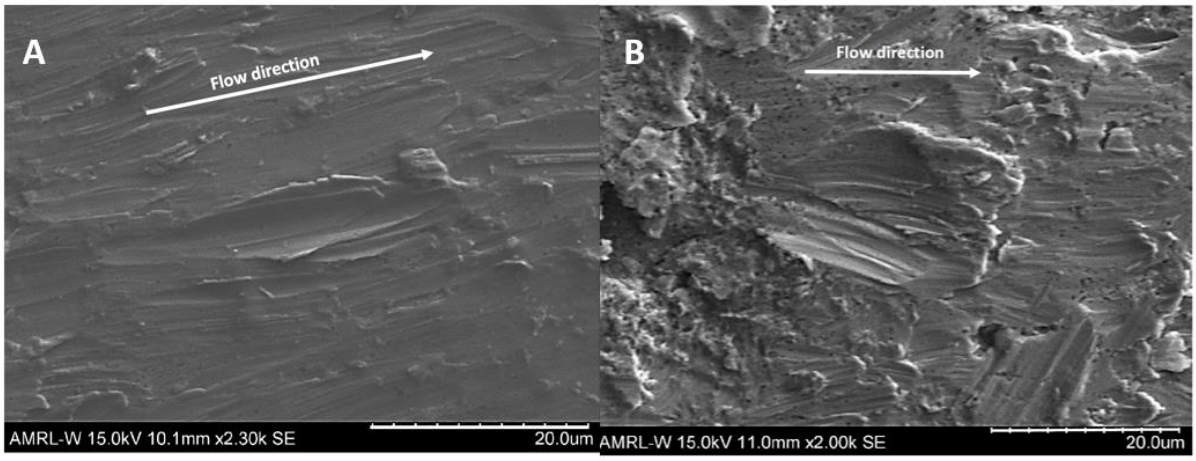

Figure 17